Allosteric threonine synthase: reorganization of the PLP site upon asymmetric activation through SAM binding to a novel site

Corine Mas-Droux, Valérie Biou, Renaud Dumas

THE JOURNAL OF BIOLOGICAL CHEMISTRY VOL. 281, NO. 8, pp. 5188–5196, February 24, 2006

Allosteric Threonine Synthase

REORGANIZATION OF THE PYRIDOXAL PHOSPHATE SITE UPON ASYMMETRIC ACTIVATION THROUGH S-ADENOSYLMETHIONINE BINDING TO A NOVEL SITE[*][S]

Received for publication, September 7, 2005, and in revised form, November 14, 2005 Published, JBC Papers in Press, November 29, 2005, DOI 10.1074/jbc.M509798200

Corine Mas-Droux[‡], **Valérie Biou**[§1], **and Renaud Dumas**[‡2]

From the [‡]*Laboratoire de Physiologie Cellulaire Végétale, Département Réponse et Dynamique Cellulaires, CNRS Commissariat à l'Energie Atomique, 38054 Grenoble, France and* [§]*Laboratoire d'Enzymologie et de Biochimie Structurales, CNRS, 91198 Gif-sur-Yvette, France*

Threonine synthase (TS) is a fold-type II pyridoxal phosphate (PLP)-dependent enzyme that catalyzes the ultimate step of threonine synthesis in plants and microorganisms. Unlike the enzyme from microorganisms, plant TS is activated by *S*-adenosylmethionine (AdoMet). The mechanism of activation has remained unknown up to now. We report here the crystallographic structures of *Arabidopsis thaliana* TS in complex with PLP (aTS) and with PLP and AdoMet (aTS-AdoMet), which show with atomic detail how AdoMet activates TS. The aTS structure reveals a PLP orientation never previously observed for a type II PLP-dependent enzyme and explains the low activity of plant TS in the absence of its allosteric activator. The aTS-AdoMet structure shows that activation of the enzyme upon AdoMet binding triggers a large reorganization of active site loops in one monomer of the structural dimer and allows the displacement of PLP to its active conformation. Comparison with other TS structures shows that activation of the second monomer may be triggered by substrate binding. This structure also discloses a novel fold for two AdoMet binding sites located at the dimer interface, each site containing two AdoMet effectors bound in tandem. Moreover, aTS-AdoMet is the first structure of an enzyme that uses AdoMet as an allosteric effector.

Threonine synthase (TS)[3] is involved in the essential amino acids pathway derived from aspartate and catalyzes the conversion of *O*-phosphohomoserine (OPH) into threonine and inorganic phosphate via a pyridoxal phosphate (PLP)-dependent reaction. Plant TS is a fascinating enzyme. Unlike bacteria and fungi, its substrate, OPH, is a branch point intermediate between the methionine and threonine pathways. Because of its specific role in the partitioning of methionine and threonine (1), plant TS, which has a low basal activity rate, has acquired an allosteric activation by *S*-adenosylmethionine (AdoMet), the end product of the methionine pathway. Indeed, previous biochemical results showed that allosteric binding of AdoMet leads to an 8-fold increase in the rate of catalysis and to a 25-fold decrease in the K_m value for OPH in the *Arabidopsis thaliana* enzyme (2). This activation is correlated with conformational modifications of the PLP environment as demonstrated by fluorescence experiments (2).

The structure of the apoform of *A. thaliana* TS (called apo-aTS hereafter) has been solved previously at 2.25 Å resolution (3). *A. thaliana* threonine synthase is a dimer with 486 amino acids/monomer. The structure of the apoenzyme shows a symmetric, compact dimer with four domains in each monomer: domain 1 (residues 1–130), domain 2 (residues 161–270), domain 3 (residues 131–160 and 271–460), and the C-terminal swap domain, thus called because it forms a structural domain with domain 2 of the other monomer (residues 461–486). The active site is located in a deep crevice at the interface of domains 2 and 3 of each monomer.

PLP-dependent enzymes catalyze a large variety of reactions, mostly on amino acid substrates. TS belongs to the family of fold-type II PLP-dependent enzymes (4). Comparison of the plant enzyme structure with the structures of the non-allosteric TS from *Thermus thermophilus* (5), *Saccharomyces cerevisiae* (6), or with the structures of other fold-type II enzymes (for example, threonine deaminase (7), *O*-acetylserine sulfhydrylase (8), or tryptophan synthase (9)) showed that all of these proteins share a common fold for domains 2 and 3, whereas domain 1 and the swap domain are specific to TS. However, the structure of the plant apo-aTS revealed an absence of electron density for PLP in the active site. In addition, several amino acids that interact with the PLP in enzymes belonging to the fold-type II family exhibit different orientations in the apo-aTS structure. Furthermore, a large loop that tops the active site and is ordered in all structures of fold-type II enzymes is disordered in the plant TS structure between residues 341 and 362. From these observations, the following three hypotheses were made. First, the apo-aTS structure previously determined might correspond to an inactive form that can only bind its PLP in a conformation unfavorable for catalysis. Second, the activator AdoMet should lead to a change in the PLP orientation to one similar to that observed in the fold-type II enzymes. Third, the above conformational modifications should promote the enzyme activation.

To check these hypotheses, we have determined the crystallographic structures of the *A. thaliana* TS in the presence of PLP and with PLP and AdoMet. Along with the structure of holoenzyme TS-PLP (called aTS hereafter), we present here the first structure of a complex between an enzyme and AdoMet as an allosteric activator (hereafter called aTS-AdoMet).

* The costs of publication of this article were defrayed in part by the payment of page charges. This article must therefore be hereby marked "*advertisement*" in accordance with 18 U.S.C. Section 1734 solely to indicate this fact.

[S] The on-line version of this article (available at http://www.jbc.org) contains supplemental Figs. 1–4 and references.

The atomic coordinates and structure factors (codes 2C2B and 2C2G) have been deposited in the Protein Data Bank, Research Collaboratory for Structural Bioinformatics, Rutgers University, New Brunswick, NJ (http://www.rcsb.org/).

[1] To whom correspondence may be addressed: Laboratoire d'Enzymologie et de Biochimie Structurales CNRS, avenue de la Terrasse, 91198 Gif-sur-Yvette cedex, France. Tel.: 33-0-1-69-82-34-81; Fax: 33-0-1-69-82-31-29; E-mail: biou@lebs.cnrs-gif.fr.

[2] To whom correspondence may be addressed: Laboratoire de Physiologie Cellulaire Végétale, Département Réponse et Dynamique Cellulaires. Commissariat à l'Energie Atomique, 38054 Grenoble, France. Tel.: 33-0-4-38-78-23-58; Fax: 33-0-4-38-78-50-91; E-mail: rdumas@cea.fr.

[3] The abbreviations used are: TS, threonine synthase; AP5, 2-amino-5-phosphonopentanoic acid; OPH, *O*-phosphohomoserine; PLP, pyridoxal phosphate; AdoMet, *S*-adenosylmethionine; aTS, *A. thaliana* threonine synthase complexed with PLP; aTS-AdoMet, *A. thaliana* threonine synthase complexed with PLP and AdoMet; tTS, *T. thermophilus* threonine synthase; r.m.s., root mean square; MES, 4-morpholineethanesulfonic acid.

EXPERIMENTAL PROCEDURES

Purification and Crystallization—A. thaliana aTS was purified as described previously (10). The purified protein was concentrated to 18 mg/ml in 20 mM HEPES-KOH, pH 7.5.

To collect the aTS data set, TS was crystallized as described in Ref. 3, with reservoirs containing 1 M LiCl, 13% (w/v) polyethylene glycol 6000, 5 mM dithiothreitol, 0.1 M MES-KOH buffer at pH 6.5 and 6 mM PLP. 2 μl of protein at 10 mg/ml were mixed with 2 μl of reservoir solution. The crystals grew for 3 weeks before they reached a size of ~500 μm. They were transferred into a solution containing 1 M LiCl, 20% (w/v) polyethylene glycol 6000, 5 mM dithiothreitol, 0.1 M MES-KOH, 10 mg/ml protein, and 6 mM PLP and incubated for 3 h before being transferred to a cryobuffer containing 10% glycerol, 1 M LiCl, 20% (w/v) polyethylene glycol 6000, 5 mM dithiothreitol, 6 mM PLP, and 0.1 M MES-KOH, pH 6.5. The crystals were flash-frozen in the cryostream. The crystals belong to the P1 space group, with unit cell dimensions of $a = 57.57$, $b = 60.94$, and $c = 76.63$ Å; $\alpha = 108.92°$, $\beta = 102.07°$, $\gamma = 107.30°$. These crystals cracked upon soaking in a solution containing AdoMet.

For aTS-AdoMet, new crystallization conditions were found using robotized screening. aTS-AdoMet was crystallized by the hanging drop vapor method at 4 °C, with reservoirs containing 10 mM $CaCl_2$, 15% (w/v) polyethylene glycol 2000 monomethyl ether, 1 mM PLP, and 100 mM BisTris, pH 6.5, buffer. aTS (8 mg/ml) was incubated with 5 mM AdoMet, and then crystallization drops were set up by mixing 2 μl of protein/AdoMet and 2 μl of reservoir solution. Crystals grew within 3–5 days and were shock-cooled in liquid N_2 in a cold room using a reservoir solution supplemented with 10% ethylene glycol a first time and 20% ethylene glycol a second time. This "progressive" method improved the diffraction. The crystals were monoclinic with a C2 symmetry. The unit cell was a = 191.9Å, b = 110.8Å, c = 152.7Å, $\alpha = \gamma = 90°$, $\beta = 89.8°$ with three dimers A-B, C-D, and E-F in the asymmetric unit and with pseudo-$P3_121$ symmetry.

Data Collection, Structure Determination, and Refinement—Data collection for aTS was performed on a lab source using a Marresearch imaging plate detector. Data were processed using XDS (11) and scaled using the SCALA program (12). X-ray data for aTS-AdoMet were collected at the European Synchrotron Radiation Facility on beamline ID14 EH1 to 2.6 Å resolution using a Marresearch CCD detector. Data were processed and scaled using the programs MOSFLM (13) and SCALA (12). The two structures were phased by molecular replacement with program MOLREP (14) using the coordinates of apo-aTS (Protein Data Bank code 1E5X). For both structures, the refinement was performed using CNS, version 1.1 (15) and the maximum likelihood target function. During the whole process, 5% of the reflections were kept apart for the R_{free} calculation. Model modifications were performed with program O (16). The refinement of aTS was straightforward. The refinement of aTS-AdoMet was done as follows. After molecular replacement, the first steps of crystallographic refinement for aTS-AdoMet consisted of a rigid body refinement at a resolution of 3 Å, with one rigid block per monomer. The R-factor was 41.4%, and the R_{free} was 41.8%. A simulated annealing refinement followed at a resolution of 2.6 Å. Harmonic non-crystallographic symmetry restraints were used with two non-crystallographic symmetry groups, each with three monomers (monomers A, C, and E in the first group and monomers B, D, and F in the second). An $F_o - F_c$ map displayed six large density peaks per dimer, which were assigned to the co-factor PLP (one in each active site) and to four AdoMet molecules (at the dimer interface). A large loop, which was not ordered in the unligated TS structure, was built in monomers A, C, and E. Thereafter, atomic positions and grouped temperature factors were refined during several cycles to reach an R-factor of 30% and an R_{free} of 35%. For the following refinement steps, individual temperature factors were introduced and an anisotropic global temperature factor and bulk solvent corrections were used. Water molecules were added at each cycle of refinement, using the WATERPICK routine in CNS. Final refinement was performed with Refmac5 (17) and TLS option using three regions per monomer for TLS calculations (18).

TABLE 1

Data collection and refinement

The numbers in parentheses indicate the value in the outer resolution shell. The R_{free} was calculated using 5% of reflections, which were kept apart from the refinement during the whole process. R.m.s., root mean square.

	aTS	aTS-SAM
Diffraction data		
Wavelength (Å)	1.54	0.934
Resolution (Å)	2.6	2.6
Space group	P1	C2
No. of reflections	51,025 (7,279)	891,931 (52,594)
No. of unique reflections	25,774 (3,698)	98,317 (14,300)
Completeness	95.5 (95.5)	99.8 (99.8)
Multiplicity	2 (2)	3.7 (3.7)
R_{sym}[a] (%)	5.4 (29.0)	8.3 (44.4)
Structure refinement		
Resolution limits (Å)	20–2.6	30–2.6
R_{factor}[b] (%)	18.5	20.6
R_{free} (%)	26.1	24.1
Total number of atoms		
No. of protein atoms	6,672	20,207
No. of solvent atoms	141	383
R.m.s. deviation		
Bond lengths (Å)	0.021	0.01
Bond angles (°)	2.6	0.97
Dihedral angles (°)	5.6	5.78
Average B factor (Å^2)		
For all atoms	26.4	59.9
For monomer A	26.5	59.8
For monomer B	26.3	60.2
r.m.s. ΔB for bonded atoms (Å^2)	1.57	1.4

[a] $R_{sym} = \Sigma_j|\langle I\rangle - I_j|/\Sigma_j\langle I\rangle$.
[b] $R_{factor} = \Sigma_j|Fo_j| - k|Fc_j|/\Sigma_j|Fo_j|$.

Structure Comparisons—For structure comparisons, unless otherwise stated, residues 36–479 from both monomers were used to calculate the best superposition using the programs LSQKAB (19) or LSQMAN (20) and superpose aTS-AdoMet and aTS dimers. The distances cited in the text correspond to the Cα–Cα distances based on this superposition. The model coordinates and structure factors were deposited at the Protein Data Bank under codes 2C2G (aTS) and 2C2B (aTS-AdoMet).

RESULTS

Overall Structure of aTS Complex—The final model of the aTS complex contains one dimer (852 amino acid residues), two PLP molecules, and 138 water molecules and was refined to an R-factor of 18.5% at 2.6 Å resolution (Table 1). The overall structure is quite similar to that of apoTS; the r.m.s. deviation between the Cα atoms is 0.55 Å. Dimer subunits are related by a non-crystallographic 2-fold axis. The Cα atoms of the two subunits were superposed with an r.m.s. deviation of 0.48 Å and similar temperature factors, indicating that the two monomers have essentially the same structure. The model is of good quality with all of the residues falling in the most favorable (85.1%), additionally allowed (14.7%), and generously allowed (0.1%) regions of the Ramachandran plot, as assessed by the PROCHECK program (21).

The surface area of the dimer interface is 7448 Å^2, which amounts to ~19% of each subunit surface area. The electron density map of aTS discloses density for amino acid residues 65–68, which were missing from the apo-aTS structure. The last amino acid residue exhibiting

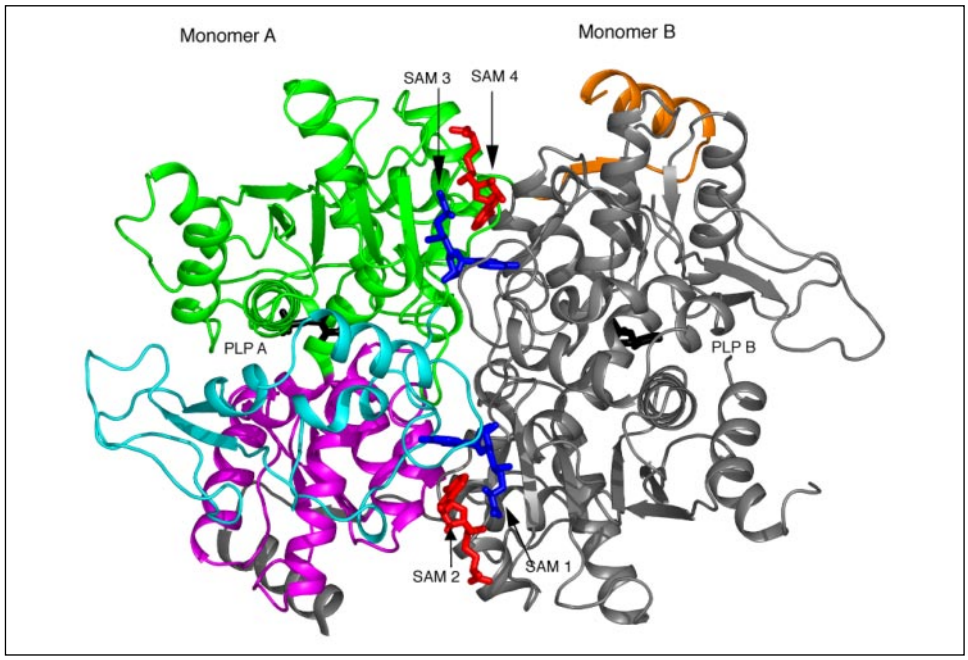

FIGURE 1. **Ribbon drawing of the aTS dimer complexed with AdoMet.** *Ribbons* of domain 1, domain 2, domain 3, and swap domain of monomer A are shown in *cyan*, *magenta*, *green*, and *orange*, respectively. The *gray ribbon* represents the monomer B. The C-terminal swap domain of each monomer interacts with domain 2 of the other monomer. The co-factor PLP is shown in *black sticks*. The four AdoMet effectors are shown at the dimer interface in *blue* (AdoMet 1 and AdoMet 3) or *red* (AdoMet 2 and AdoMet 4) *sticks*. All protein representations were done using the program PYMOL (www.pymol.org). *SAM*, AdoMet.

density is Gly-480. Similarly to apo-aTS, the N terminus residues are only partly ordered; residues 11–21 and 29 onward in monomer A and residues 21–25 and 32 onward in monomer B could be traced. The $F_o - F_c$ electron density map shows, inside the active site of each monomer, a PLP co-factor bound to Lys-163 via a Schiff base. The active site conformation of aTS is different compared with those observed in the structure of non-allosteric TS from *T. thermophilus* (5) or *S. cerevisiae* (6). In addition, the PLP orientation inside the aTS catalytic site is completely different compared with all other known enzyme structures belonging to the fold-type II PLP-dependent family. Also, loop 341–362 involved in the stabilization of PLP in TS from microorganisms is disordered in the aTS, as previously observed for the structure of apo-aTS.

Overall Structure of aTS-AdoMet Complex—The final model of the aTS-AdoMet complex contains six monomers that clearly correspond to three functional dimers, with an interface involving the same residues as in apo-aTS. The model comprises 2598 amino acid residues, 6 PLPs, 12 AdoMets, and 383 water molecules in the asymmetric unit and was refined to an R-factor of 20.6% at 2.6 Å resolution (Table 1). The main chain atoms of the three dimers were superposed with an r.m.s. deviation of 0.15 Å, indicating that the three dimers have the same structure. The model of aTS-AdoMet is also of good quality, with all of the residues falling in the most favorable (87.2%), additionally allowed (12.3%), and generously allowed (0.4%) regions of the Ramachandran plot. Only two residues per dimer are in the disallowed region. These residues (47 and 48 in monomer A) are located in a tight loop and show a well defined density.

The structure of aTS co-crystallized with PLP and its allosteric effector AdoMet revealed the presence of four AdoMet molecules located at the dimer interface (Fig. 1). The surface area of the dimer interface is 7006 Å^2, which amounts to ~18% of the subunit surface area. This value is similar to the one determined for aTS, indicating that AdoMet binding does not make a significant change to the surface involved in the dimer interface. However, superposition of the Cα atoms of the aTS-AdoMet and the aTS dimers give an overall r.m.s. deviation of 1.54 Å and a maximum deviation of 5.6 Å, indicating that important changes do occur upon AdoMet binding. Interestingly, the Cα atoms of monomers A and B of aTS-AdoMet were superposed with the corresponding monomers of aTS, with an r.m.s. deviation of 1.51 and 0.92 Å, respectively, showing that the dimer of the aTS-AdoMet is asymmetric and that monomer B is more similar to aTS than to monomer A. Therefore, AdoMet induces different conformational changes to monomers A and B. These important modifications upon AdoMet binding led to the reorganization of only one active site. Thus, aTS-AdoMet structure consists of an asymmetric dimer in which one PLP in monomer B has an orientation similar to that found in the aTS structure, whereas the one in monomer A has an orientation similar to that found in the crystal structure of TS from microorganisms and all other related structures. This difference is observed in all three dimers in the asymmetric unit, and the rest of the discussion will focus on the A-B dimer only.

PLP Binding Site of aTS—PLP binding does not alter the main chain atoms of residues involved in the catalytic pocket in aTS as compared with apo-aTS. However, upon PLP binding, the side chain of Asn-296 moves away from the co-factor by 2.9 Å. Fig. 2*A* shows PLP interactions inside the catalytic pocket. The phosphate group of PLP interacts with Ser-191 and Thr-195 via two hydrogen bonds. The pyridine ring is sandwiched between Arg-267 and Asn-296. In addition, it is surrounded on the N1 side by Ser-261 and on the O3′-side by residues Lys-163 (with which it forms a Schiff base), Gln-271, and Asn-299. Both hydrophobic and polar contacts are formed. Residues that interact with the PLP in this new manner are not specific to plant sequences, but they are shared by other TS sequences, as well as by other fold-type II enzymes (see sequence alignment in supplemental Fig. 1). However, the orientation of the residues and position of PLP in the aTS structure is unique for an enzyme of the fold-type II PLP-dependent family.

The Two PLP Binding Sites of aTS-AdoMet—Upon AdoMet binding, monomer A undergoes a large active site rearrangement, whereas the active site and PLP orientation of monomer B remains unchanged. The reorganization in monomer A consists of a PLP swing and a shift of loops 190–195, 260–264, and 294–299, with a maximum displacement of Thr-192 and Asn-296 by 2.53 and 3.05 Å, respectively (Fig. 2, compare *A* and *B*). In addition, the electron density becomes well defined for the large loop 341–362, which is stabilized and interacts with residues of the catalytic pocket. However, the PLP does not form any electrostatic interaction with residues from this loop (the closest residue is Ala-356,

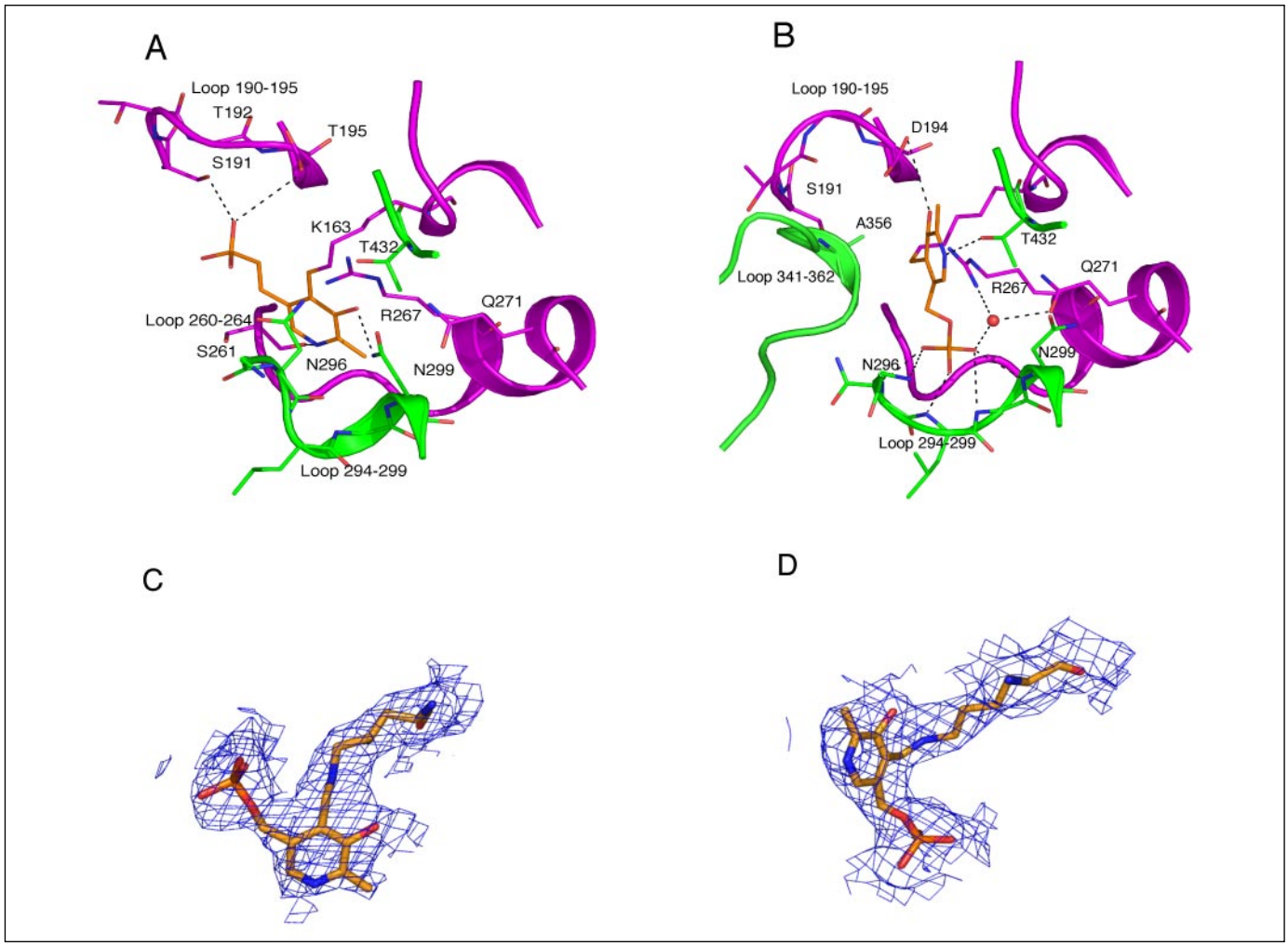

FIGURE 2. **Active site and PLP orientation.** *A*, interactions of PLP inside the active site of aTS. *B*, interactions of PLP inside the active site of monomer A of aTS-AdoMet. Domains 2 and 3 are shown in *magenta* and *green*, respectively. PLP is shown in *orange stick*, and the water molecule is represented as a *red sphere*. *Dotted lines* show interaction <3.3 Å between PLP and residues of the active site. AdoMet binding induces conformational changes leading to the reorganization of one active site with a PLP orientation similar to that observed in non-allosteric TS. *C* and *D*, $2mF_o - DF_c$ electron density maps around the PLP molecules for aTS and aTS-AdoMet monomer A, respectively. Maps are traced at 1 standard deviation.

whose Cβ atom is 3.5 Å away from the PLP pyridine ring). The movement of the PLP involves a 150° rotation around the C5–C5A bond, leading to a conformation similar to that observed in the TS structures from microorganisms. As described in Fig. 2*B* and supplemental Fig. 2, most of the residues involved in the interaction of PLP in its new position for monomer A of aTS-AdoMet were also involved in the binding of PLP in aTS. However, the interaction pattern with these residues is completely reorganized. As observed for other fold-type II enzymes, the phosphate group makes four hydrogen bonds with the main chain nitrogens of the semicircular loop 295–299. In addition, Arg-267 and Gln-271 interact with the phosphate group via a water molecule. The pyridine ring is surrounded by loop 191–195 on the O3′-side and by residues 431–433 on the N1 side. Thus, Asp-194 and Thr-432 make hydrogen bonds with O3′ and N1, respectively. In addition, the pyridine ring is surrounded by Phe-162 and Ala-356.

AdoMet Binding Sites—Fig. 3 shows details of the AdoMet binding sites. The crystal structure of aTS-AdoMet contains two activator binding sites (1 and 2) located at the dimer interface with two AdoMet molecules in each site. As shown in Fig. 1, we have called site 1 the one that holds AdoMet 1 and 2, whereas site 2 holds AdoMet 3 and 4 (Fig. 3*A*). AdoMet 1 and 3 are most deeply buried in the dimer interface, whereas AdoMet 2 and 4 are more exposed to the solvent (Fig. 1). Moreover, all atoms from AdoMet 1 show a well defined electron density, whereas a gap can be observed between the sulfonium and the adjacent carbon of the methionine moiety of AdoMet 2, 3, and 4 (Fig. 3*C*). In each binding site, the two AdoMet molecules are in close proximity to each other and have two different conformations, whereas a superposition of sites 1 and 2 shows that both corresponding AdoMets have similar conformations.

Each AdoMet is stabilized by amino acids from both monomers. One side of each AdoMet binding site is made of loop 96–106 and region 120–130 belonging to domain 1 from one monomer, whereas the other side is formed by region 131–154 belonging to domain 3 from the other monomer. Thus AdoMet 1 and 2 make interactions with domain 1 of monomer A and with domain 3 of monomer B. Symmetrically, AdoMet 3 and 4 are stabilized by domain 1 of monomer B and domain 3 of monomer A (Fig. 3*A*). The main stabilizing interactions for AdoMet 1 and AdoMet 3 are hydrogen bonds formed by the adenosine and the ribose with residues from both monomers, whereas their methionine moiety is in close proximity to the Trp-150 side chain and to AdoMet 2 and AdoMet 4 ribose, respectively (the main chain moiety of AdoMet 1 is within 3.5 Å of distance from the AdoMet 2 ribose oxygen) (Fig. 3, *B* and *D*). AdoMet 2 and AdoMet 4 are mainly stabilized via interactions

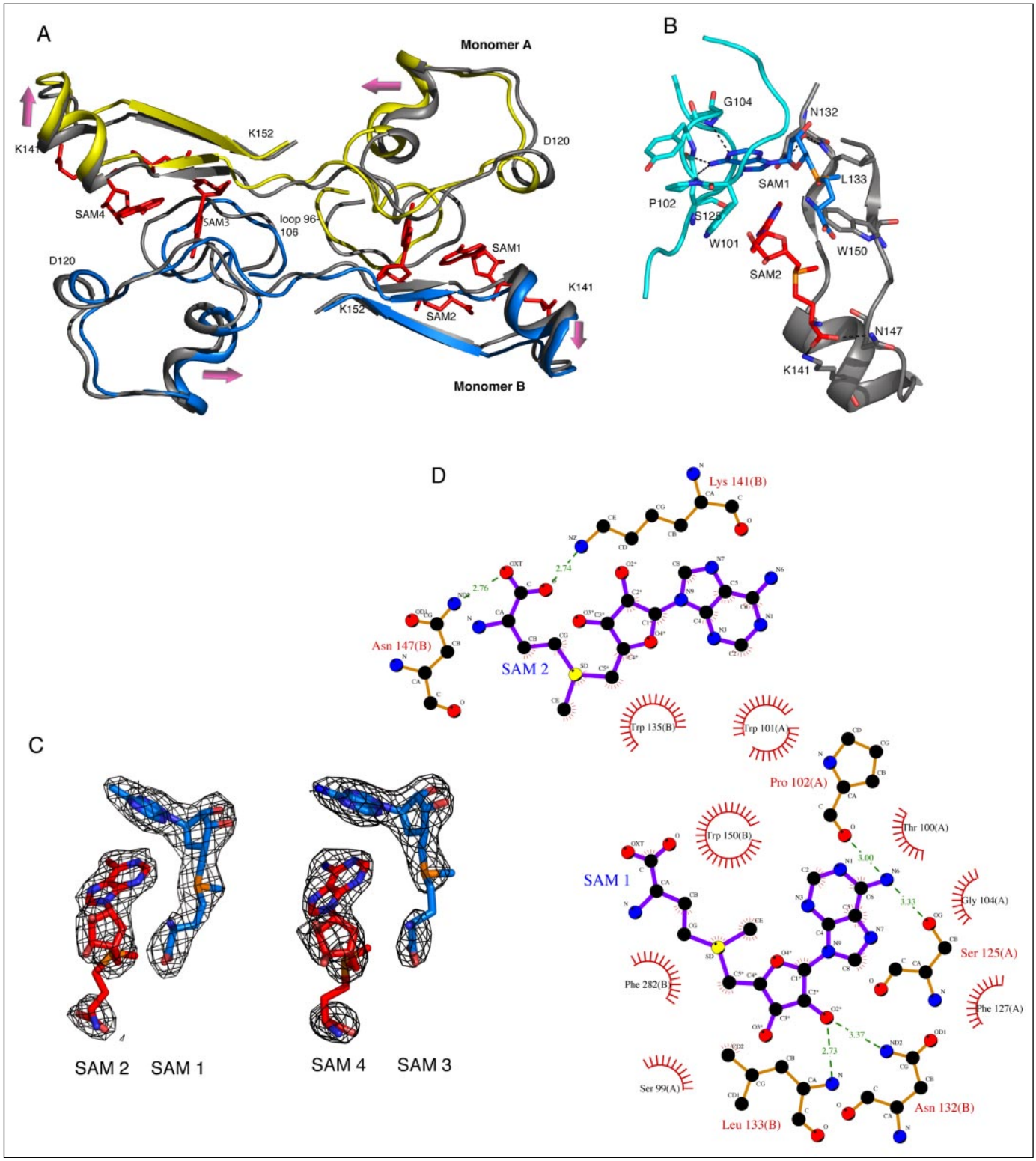

FIGURE 3. **Detailed view of the AdoMet binding sites.** *A*, sliding of monomers A and B along the dimer interface upon AdoMet binding. Effector binding sites are indicated and AdoMet molecules are shown in *red*. Site 1 comprises AdoMet 1 and 2, and site 2 comprises AdoMet 3 and 4. aTS is shown in *gray*, whereas monomers A and B of aTS-AdoMet are shown in *yellow* and *blue*, respectively. The *arrows* indicate movement directions. *B*, structure of the AdoMet binding site 1 showing that both monomers are involved in the interaction with AdoMet molecules inside each AdoMet binding site. Domain 1 of monomer A and domain 3 of monomer B are shown in *cyan* and *gray*, respectively. AdoMet 1 and 2 are shown in *blue* and *red sticks*, respectively. *Dotted lines* show interactions between AdoMet molecules and residues of the binding site 1. *C*, electron density associated with the four AdoMet activator molecules. The SIGMAA electron density map ($2mF_o - DF_c$) was calculated using the REFMAC5 parameters and the CCP4 program suite. AdoMet 1 and 2 from binding site 1 and AdoMet 3 and 4 from site 2 are shown in *blue* and *red*, respectively. *D*, schematic representation of the interactions of AdoMet 1 and 2 molecules in site 1. The figure was done using the program LIGPLOT (28). *SAM*, AdoMet.

of their adenosine ring with two tryptophan side chains (Fig. 3, *B* and *D*). Trp-101 is stacked against the adenine ring, whereas Trp-150 is perpendicular to it, the closest atoms being 3.6 Å apart.

Sites 1 and 2 present very similar interactions with AdoMet molecules. However, although AdoMet 2 and 4 have equivalent positions, their interactions with the protein are not identical. In particular, the

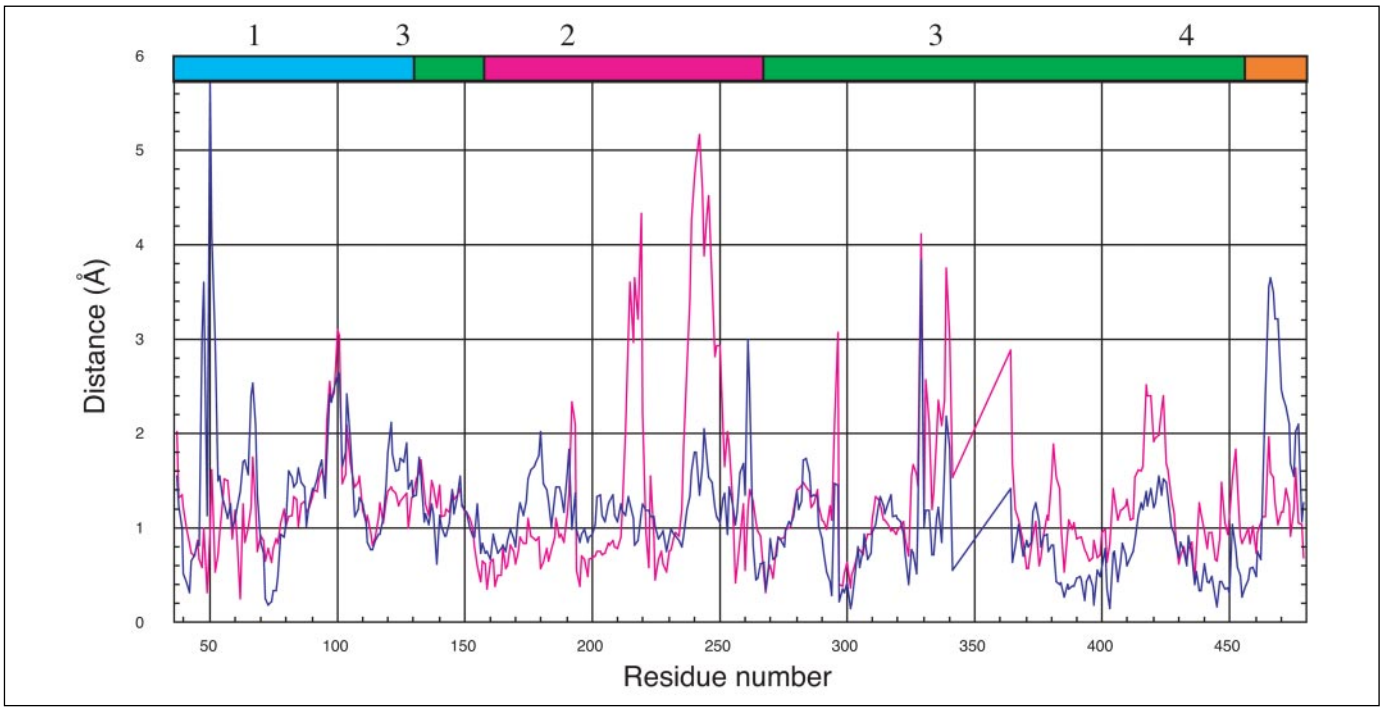

FIGURE 4. **Conformational changes upon AdoMet binding.** This graph shows the deviations in the corresponding Cα atoms between aTS and aTS-AdoMet for monomer A (in *pink*) and monomer B (in *blue*). The horizontal axis corresponds to the residue number. The whole dimer was included for the superposition. The *cyan*, *pink*, *green*, and *orange* frames correspond to domains 1, 2, 3 and the swap domain, respectively. This graph indicates that AdoMet binding induces different conformational changes on the two monomers.

AdoMet 2 methionine carboxyl makes an electrostatic interaction with Lys-141 and Asn-147 of monomer B (Fig. 3*D*), whereas the AdoMet 4 methionine moiety interacts only with Lys-141 of monomer A.

AdoMet Induces Asymmetric Conformational Changes—Fig. 3*A* shows that AdoMet binding induces a sliding of both monomers along the dimer interface. In particular, loops 96–106 of both monomers come closer to each other. A global movement, corresponding to a rotation of domain 2 toward and of domain 3 away from the interface is a consequence of this interface sliding (see Fig. 5).

Fig. 4 shows the displacements of the Cα atoms between aTS-AdoMet and aTS, as calculated by LSQKAB (19) for both monomers. As shown on this figure, AdoMet binding induces important asymmetric conformational modifications (illustrated by peaks in Fig. 4). Monomer A presents three main peaks for domain 2 and three main peaks for domain 3, whereas monomer B shows only one large peak located at the swap domain, which forms a structural unit with domain 2 of monomer A (Fig. 4).

As shown on Figs. 5 and 6, these modifications consist of two large, asymmetric changes. The first one corresponds to the rotation of a β-sheet formed by strands β6, β7 of monomer A domain 2, and β13 of monomer B swap domain. This sheet, along with the associated loops (216–219 and 237–240) and helices α11 and α21, rotate by an angle of 16° around an axis passing through residues A210, A233, and B460 (Fig. 6*A*). The second asymmetric change is the stabilization of the large loop 341–362 in monomer A above the active site (Fig. 5).

All movements described above contribute to a reorganization of the active site of monomer A only (see the animation in supplemental Fig. 3). As a consequence of AdoMet binding, the accessible surface area calculated using the program AREAIMOL (22) of the active site of monomer A is reduced from 890 Å^2 (aTS) to 514 Å^2 for (aTS-AdoMet). The closure of the active site cleft induced by AdoMet is obvious on supplemental Fig. 4, which shows the comparison between the surface of monomers in aTS and aTS-AdoMet.

DISCUSSION

The structure of aTS discloses a PLP bound in an inactive conformation. The structure of aTS-AdoMet shows that AdoMet binding triggers the rotation of one PLP to its active conformation along with the reorganization of the active site. The following discussion will focus on how TS is able to perform this task via plant-specific active site conformational changes and the AdoMet binding site.

Active Site Comparison between A. thaliana and Other Threonine Synthases—*T. thermophilus* (tTS, Protein Data Bank code 1UIN (5)) and *S. cerevisiae* (sTS, Protein Data Bank code 1KL7 (6)) threonine synthase structures show an active site and a PLP binding similar to those of other fold-type II PLP-dependent enzymes represented by tryptophan synthase (9). However, the conformations of the active site residues of the plant apo-aTS or aTS are different from those structures. As a result, the cofactor in the structure of aTS cannot bind in the same orientation. In particular, in aTS, the position of loop 294–298 prevents the PLP phosphate group from binding in an orientation similar to that of other PLP enzymes. The comparison between aTS and tTS complexed with a substrate analogue, 2-amino-5-phosphopentanoic acid (AP5) (tTS-AP5, Protein Data Bank code 1V7C (5)), shows that the PLP in aTS is in the substrate site. In particular, the pyridine cycle of the PLP takes the place of the substrate phosphate. This unusual PLP orientation partly blocking the substrate site explains the low affinity of aTS for its substrate and the low k_{cat} measured in the absence of AdoMet (2). The structure superposition shows that the inactive orientation of PLP would bring steric clashes with at least two amino acids in the *T. thermophilus* structure (Asn-188, equivalent to Asn-296 in *A. thaliana*, and Ser-155, equivalent to Ser-262 in *A. thaliana*). Therefore, the *T. thermophilus* structure is not compatible with the inactive conformation of PLP.

In agreement with our hypotheses described in the Introduction and with biochemical experiments indicating that AdoMet induces a modification of PLP fluorescence (2), our crystallographic results show that

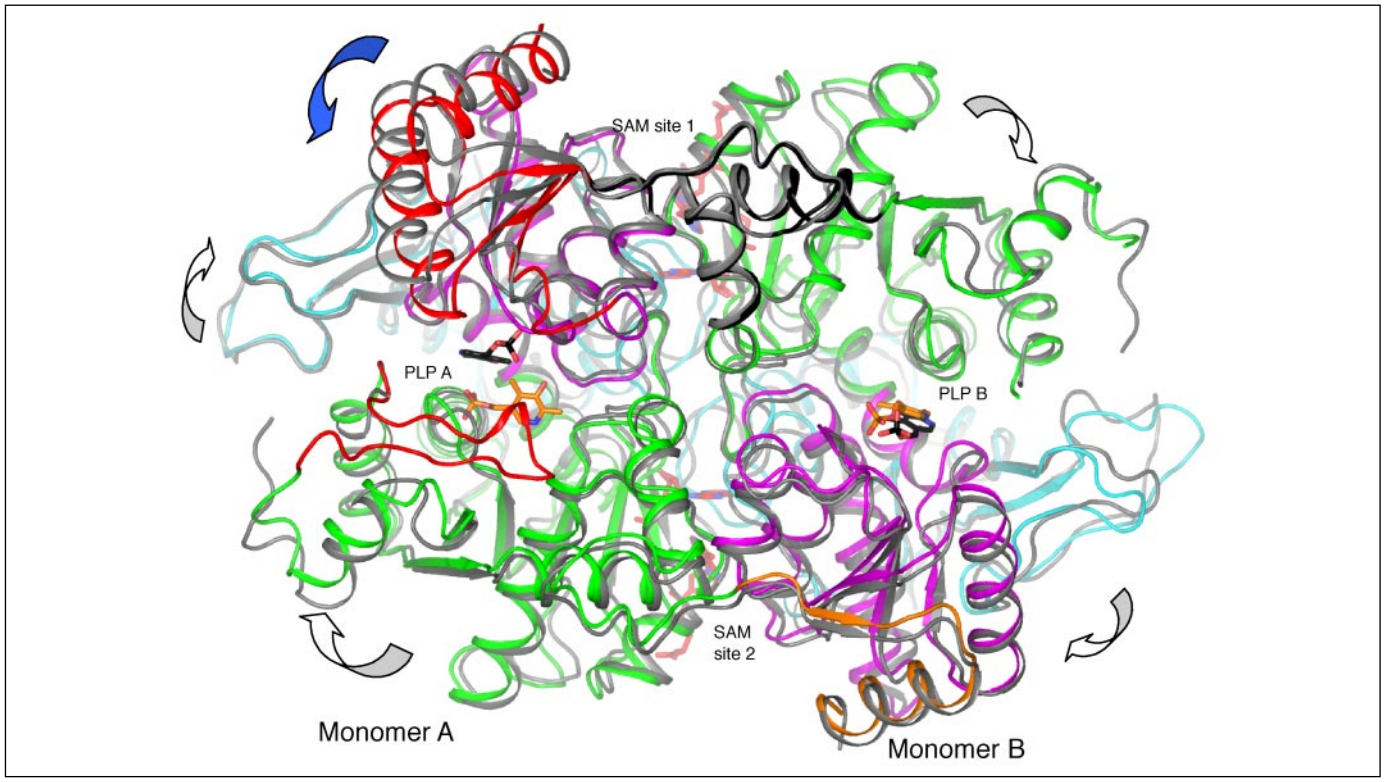

FIGURE 5. **Superposition of aTS and aTS-AdoMet showing conformational changes induced by AdoMet binding.** aTS is shown in *gray*, whereas domains 1, 2, 3, and swap domain of aTS-AdoMet are shown in *cyan*, *magenta*, *green*, and *orange*, respectively. Domain 2 from monomer A along with the swap domain from monomer B (shown in *red*) undergo a large movement (indicated by a *blue arrow*). The rigid block is shown in *black*. The large loop (341–362) is shown in *red*. *Gray arrows* show the global dimer movement. *SAM*, AdoMet.

AdoMet binding induces the reorganization of the PLP binding site. Most of the residues involved in PLP stabilization in the activated monomer A of aTS-AdoMet are conserved in all TS sequences. Loop 294–298 is less conserved in terms of sequence, but the interaction with the phosphate group occurs via the main chain, and its change between active and inactive conformation is probably helped by plant-specific Gly-294. Once the PLP is in its active position, the active site conformation is the same as for all enzymes in the family, and the reaction is likely to proceed in the same way as for non-allosteric TS enzymes (5, 23).

Surprisingly, the conformation of loops 190–194 and 260–264 in aTS-AdoMet monomer A is more similar to that of tTS-AP5 than to that observed in tTS in the absence of the substrate analogue. These loops are involved in substrate stabilization in tTS-AP5. The active site of aTS-AdoMet monomer A is thus ready to host the substrate with a better affinity than is empty tTS. The PLP and the substrate can bind optimally, and the reaction will be more efficient than for aTS. This is a likely explanation for the measured increase in k_{cat} upon AdoMet binding (2). In summary, plant threonine synthase has invented an additional inactive PLP binding site using the same residues, where the PLP plays the role of a reversible inhibitor.

The AdoMet Binding Sites Are Plant-specific and Have a Unique Fold—The structure of the *A. thaliana* enzyme reveals that the plant TS dimer binds four AdoMet molecules (Fig. 1). This observation agrees with the results of kinetic experiments, which show that the curve of enzyme activity as a function of AdoMet concentration (at low OPH concentration) can be fitted by a cooperative equation with a Hill number of 2.9 (2). Further support is given by previous spectrometric experiments, which showed that the progressive addition of AdoMet induces a two-step modification of PLP fluorescence at 489 nm of the plant enzyme. First, low AdoMet concentration triggers a decrease in fluorescence, and further addition triggers an increase that can be fitted by a cooperative equation with a Hill number of 3 (2). These biochemical results suggested (i) a sequential AdoMet binding and (ii) that plant TS binds more than three AdoMet molecules. From the present structure, we propose that the more-buried AdoMet 1 and 3 molecules bind first, followed by AdoMet 2 and 4.

Supplemental Fig. 1 shows a structure-based sequence alignment between the TS of plants and microorganisms. Regions involved in AdoMet binding are highly conserved in plant sequences but not in microorganisms. The sequence alignment shows that similarity between plant and microorganism enzymes starts just after the second AdoMet site. The superposition between the aTS and yeast structures confirms that loop 94–106 does not exist in the yeast structure, and the *T. thermophilus* sequence starts at the equivalent of residue 103 in *A. thaliana*. In addition, structure superposition shows that helix α6 holding Lys-141 and Asn-147 has a different orientation in *T. thermophilus* and would be unable to stabilize the AdoMet 2 methionine carboxylate. Despite a very different sequence, monomeric yeast TS shows a structural equivalent of residues 130–145, representing half of an AdoMet binding site. However, the rest of the dimer interface is missing.

AdoMet-binding proteins display a variety of binding folds. Accordingly, the AdoMet binding site of aTS shows a topology different from those observed in other AdoMet-binding proteins of known structure, such as methyl transferases (24), AdoMet radical-dependent enzymes (biotin synthase from *Escherichia coli* (25), and coproporphyrinogen III oxidase HemN from *E. coli* (26)) or Met repressor MetJ (27). The only structure showing a site with two AdoMet molecules in contact is that of HemN, but the relative orientation and AdoMet binding fold are very different from those of aTS-AdoMet.

The structure of aTS complexed to its activator AdoMet contains, therefore, a new plant-specific AdoMet binding fold. The tandem binding mode may be a way to stabilize the AdoMet molecules via intermo-

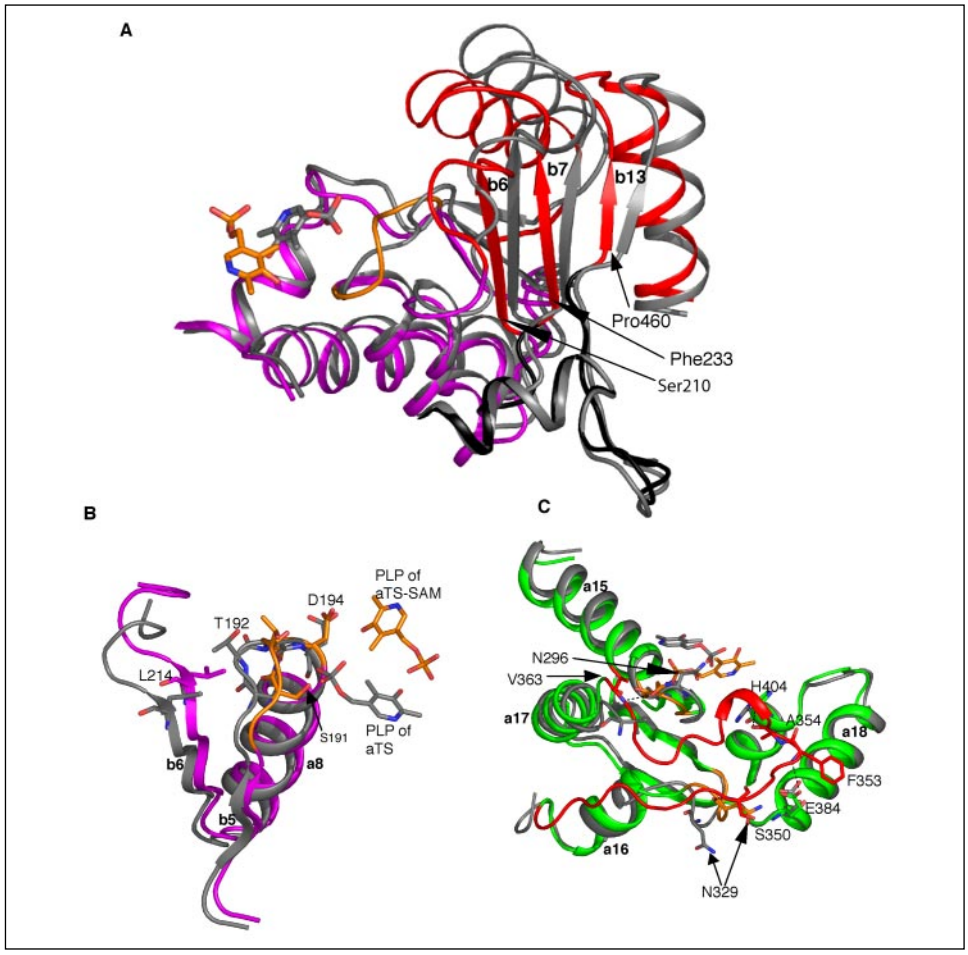

FIGURE 6. **Detailed views of conformational changes around the active site upon AdoMet (*SAM*) binding (the global *color coding* is the same as that used in Fig. 5).** *A*, strands β6A, β7A, β13B, and loop 216–219 (in *red*) undergo a large shift around a rigid block (in *black*). *B*, this shift induces a rotation of Thr-192 toward the active site and subsequent reorientation of Ser-191, Gly-193, and Asp-194. *C*, organization of the large loop 341–362 (in *red*) correlated with interaction with residues Asn-296, Asn-329, Glu-384, and His-404. β-strands (*b*) and α-helices (*a*) are labeled.

lecular contacts. Site-directed mutagenesis experiments are underway to explore the individual role of each AdoMet site.

Mechanism by which AdoMet Activates One Active Site in the Dimer—As was shown under "Results," despite very similar interactions, the AdoMet sites are slightly different, as the AdoMet 2 methionine interacts with both Lys-141 and Asn-147 of monomer B, whereas AdoMet 4 methionine interacts only with Lys-141 of monomer A (Fig. 3*D*). The interaction of AdoMet 2 with Lys-141 and Asn-147 contributes to the stabilization of residues 137–149 of monomer B. As a consequence, the higher stability of site 1 with respect to site 2 would lead to different changes in each monomer.

Fig. 5 shows a superposition of aTS and aTS-AdoMet structures and serves as a basis for proposing a mechanism for the large changes observed in monomer A domain 2. Observation of the whole structure shows homogeneous rotation for domains 2B and 3A by contrast to heterogeneous movement for domains 2A and 3B (Fig. 5).

Those heterogeneous movements observed in domains 2A and 3B may be correlated to the more stable AdoMet site 1. Indeed, a rigid block shown in *black* on Fig. 5 and formed by three interacting regions (residues 221–234 from monomer A; 382–403 and 436–460 from monomer B) is situated around site 1. It is located at the N terminus ends of the rotated β-sheet strands described under "Results." This region shows a low displacement amplitude upon AdoMet binding. The rigid block seems to act as a lever arm to transform the global movement of the dimer into a large, local rotation of this region (Fig. 6*A*). This rotation leads to strand β6 (210–215) undergoing a large shift that brings Leu-214 to within 1.3 Å from the Thr-192 location in aTS (Fig. 6*B*). This steric clash probably pushes Thr-192 to rotate by 45° toward the active site, thus forcing its neighboring residues Ser-191, Gly-193, and Asp-194 to reorient and form the active site. Ser-191 is now too close to the PLP phosphate group in aTS and thus forces the PLP to change its position (Fig. 6*B*).

The largest change in domain 3 of monomer A is the ordering of the large loop (341–362) (Figs. 5 and 6*C*). The mechanism of this ordering is difficult to understand from the present structures. As a consequence of the loop ordering, loop 327–330 and helix α16 at the N-terminal side of loop 341–362 undergo a large movement that allows Asn-329 to form new interactions with the side chain of Glu-384 and with the main chain of residues 350 and 351. These and other interactions shown on Fig. 6*C* are very important in the stabilization of the N terminus region of the loop. The large loop reorganization in monomer A is correlated with a shift of loop 294–298 to accommodate the PLP phosphate in the active conformation (Fig. 6*C*). Loop 294–298 gets twisted, because strand β9 and helix α15 on either side undergo movements of different amplitudes (1.1 *versus* 0.8 Å). This new conformation is stabilized by interactions made by the Asn-296 side chain with the Val-363 main chain right after loop 341–362 and with Ser-262. Even though all residues of the large loop have a well defined electron density, their average B-factor is 74 $Å^2$, whereas the average B-factor of monomer A is 60 $Å^2$ on all atoms. This difference does not exist in the *T. thermophilus* structure, where the large loop has B-factors in the same range as the rest of the structure. Therefore, the loop in aTS-AdoMet may not be completely stabilized in its active form. Contrary to monomer A, due to the homogeneous movement of its environment in monomer B, loop 294–298 cannot become twisted. In addition, the lower amplitude of helix α16 movement does not allow stabilization of loop 341–362, and the PLP stays in its inactive position.

In summary, AdoMet binding at the more stable site 1 triggers the rotation of domain 2 via a rigid block located around site 1. This rotation stabilizes half of the active site of domain A. The other half, corresponding to domain 3, is stabilized through ordering of loop 341–362 and neighboring loops.

A Possible Role of the Substrate in Second Monomer Activation—Kinetic studies showed that an increase in substrate concentration enhances the affinity of the protein for AdoMet (2). Moreover, PLP fluorescence studies have shown that the PLP environment change, and thus the protein conformational modification triggered by AdoMet binding, is slow in the absence of substrate (~300 s) but accelerates when OPH is added (2). The present structural study shows that AdoMet triggers an asymmetric activation in the absence of substrate, where a single active site is in an activated conformation ready to receive and transform the substrate. The binding of the substrate in the active site of monomer A might induce new conformational changes that could trigger monomer B activation. Indeed, a comparison between tTS with and without the substrate analogue shows that substrate binding triggers a closure of the active site via a large shift in domain 2 due to movements of residues involved in AP5 binding (5). Domain 2 β-sheet acts as a hinge by which the top of domain 2 plus the monomer B swap domain move by a large amplitude. The movement of rotation around the β-sheet leading to a closure of the active site in tTS is similar to that observed in monomer A in aTS-AdoMet (as seen in Fig. 6*A*), but it is larger in *T. thermophilus*. Substrate binding in the monomer A active site might trigger the same effect, *i.e.* amplify domain 2 conformational change and help monomer B activation. Crystallization of aTS in the presence of PLP, AdoMet, and a substrate analogue is underway to check this new hypothesis.

In summary, the PLP in the active site of aTS has an orientation that has never been observed in any known fold-type II enzyme. This corresponds to an inactive conformation. The structure of aTS-AdoMet shows that AdoMet binding induces large, asymmetric, conformational modifications leading to the reorganization of the active site and its PLP, as observed in all fold-type II enzymes, in one monomer only. The present work shows in detail how AdoMet, by binding to a plant-specific dimer interface, activates threonine synthase by triggering its PLP co-factor rotation and active site stabilization. The aTS-AdoMet complex discloses a novel fold for two AdoMet binding sites located at the dimer interface, with two AdoMet effectors in each active site. This asymmetric structure may be that of a trapped intermediate, which would exist only transiently in the cell, due to the high affinity of TS for OPH when AdoMet is bound.

Acknowledgments—We thank Drs. Gilles Curien and Stéphane Ravanel, Prof. Roland Douce (Laboratoire de Physiologie Cellulaire Végétale, Grenoble, France), Drs. Andy Thompson and Pierre Legrand (Synchrotron SOLEIL, Gif-sur-Yvette), and Dr. Jean-Luc Ferrer (Institut de Biologie Structurale de Grenoble) for helpful discussions and critical reading of the manuscript. We are grateful to the staff at beamline ID14-EH1 (European Synchrotron Radiation Facility, Grenoble, France).

REFERENCES

1. Curien, G., Ravanel, S., and Dumas, R. (2003) *Eur. J. Biochem.* **270,** 4615–4627
2. Curien, G., Job, D., Douce, R., and Dumas, R. (1998) *Biochemistry* **37,** 13212–13221
3. Thomazeau, K., Curien, G., Dumas, R., and Biou, V. (2001) *Protein Sci.* **10,** 638–648
4. Schneider, G., Käck, H., and Y., L. (2000) *Structure* (*Camb.*) **8,** R1–R6
5. Omi, R., Goto, M., Miyahara, I., Mizuguchi, H., Hayashi, H., Kagamiyama, H., and Hirotsu, K. (2003) *J. Biol. Chem.* **278,** 46035–46045
6. Garrido-Franco, M., Ehlert, S., Messerschmidt, A., Marinkovic, S., Huber, R., Laber, B., Bourenkov, G. P., and Clausen, T. (2002) *J. Biol. Chem.* **277,** 12396–12405
7. Gallagher, D. T., Gilliland, G. L., Xiao, G., Zondlo, J., Fisher, K. E., Chinchilla, D., and Eisenstein, E. (1998) *Structure* (*Camb.*) **6,** 465–475
8. Burkhard, P., Rao, G. S., Hohenester, E., Schnackerz, K. D., Cook, P. F., and Jansonius, J. N. (1998) *J. Mol. Biol.* **283,** 121–133
9. Hyde, C. C., Ahmed, S. A., Padlan, E. A., Miles, E. W., and Davies, D. R. (1988) *J. Biol. Chem.* **263,** 17857–17871
10. Curien, G., Dumas, R., Ravanel, S., and Douce, R. (1996) *FEBS Lett.* **390,** 85–90
11. Kabsch, W. (1993) *J. Appl. Crystallogr.* **26,** 795–800
12. Evans, P. R. (1997) in *Recent Advances in Phasing*, pp. 97–102, Daresbury Laboratory, Warrington, UK
13. Leslie, A. G. W. (1992) *Joint CCP4 and ESF-EAMCB Newsletter on Protein Crystallography* **26**
14. Vagin, A., Teplyakov, A. (1997) *J. Appl. Crystallogr.* **30,** 1022–1025
15. Brunger, A. T., Adams, P. D., Clore, G. M., DeLano, W. L., Gros, P., Grosse-Kunstleve, R. W., Jiang, J. S., Kuszewski, J., Nilges, M., Pannu, N. S., Read, R. J., Rice, L. M., Simonson, T., and Warren, G. L. (1998) *Acta Crystallogr. Sect. D. Biol. Crystallogr.* **54,** 905–921
16. Jones, T. A., Zou, J. Y., Cowan, S. W., and Kjeldgaard, M. (1991) *Acta Crystallogr. Sect. A* **47,** 110–119
17. Murshudov, G. N., Vagin, A. A., and Dodson, E. J. (1997) *Acta Crystallogr. Sect. D.* **53,** 240–255
18. Winn, M. D., Isupov, M. N., and Murshudov, G. N. (2001) *Acta Crystallogr. Sect. D.* **57,** 122–133
19. Kabsch, W. (1976) *Acta Crystallogr. Sect. A* **32**, 922–923
20. Kleywegt, G. J., and Alwyn Jones, T. (1997) *Methods in Enzynology* (Carter, C. W., Jr., and Sweet, R. M., eds) Vol. 277, pp. 525–545, Academic Press
21. Laskowski, R., MacArthur, M., Moss, D., and Thornton, J. (1993) *J. Appl. Crystallogr.* **26,** 283–291
22. Lee, B., and Richards, F. M. (1971) *J. Mol. Biol.* **55,** 379–400
23. Laber, B., Gerbling, K. P., Harde, C., Neff, K. H., Nordhoff, E., and Pohlenz, H. D. (1994) *Biochemistry* **33,** 3413–3423
24. Martin, J. L., and McMillan, F. M. (2002) *Curr. Opin. Struct. Biol.* **12,** 783–793
25. Berkovitch, F., Nicolet, Y., Wan, J. T., Jarrett, J. T., and Drennan, C. L. (2004) *Science* **303,** 76–79
26. Layer, G., Moser, J., Heinz, D. W., Jahn, D., and Schubert, W. D. (2003) *EMBO J.* **22,** 6214–6224
27. Somers, W. S., and Phillips, S. E. V. (1992) *Nature* **539,** 387–393
28. Wallace, A., Laskowski, R., and Thornton, J. (1995) *Protein Eng.* **8,** 127–134

Allosteric Threonine Synthase: REORGANIZATION OF THE PYRIDOXAL PHOSPHATE SITE UPON ASYMMETRIC ACTIVATION THROUGH S-ADENOSYLMETHIONINE BINDING TO A NOVEL SITE

Corine Mas-Droux, Valérie Biou and Renaud Dumas

J. Biol. Chem. 2006, 281:5188-5196.
doi: 10.1074/jbc.M509798200 originally published online November 29, 2005